Gold Bull (2013) 46:47–56
DOI 10.1007/s13404-013-0080-2

ORIGINAL PAPER

Subcellular localization of gold nanoparticles in the estuarine bivalve *Scrobicularia plana* after exposure through the water

Yolaine Joubert · Jin-Fen Pan · Pierre-Emmanuel Buffet · Paul Pilet · Douglas Gilliland · Eugenia Valsami-Jones · Catherine Mouneyrac · Claude Amiard-Triquet

Published online: 14 February 2013

Abstract Nanoparticles are extensively used particularly in biomedical and industrial applications. Because of their colloidal stability, gold nanoparticles (AuNPs) are suspected being persistent in aquatic ecosystem. Thus, the potential toxicity of gold nanoparticles is addressed by using a bivalve model *Scrobicularia plana*. Using AuNPs in a range of sizes (5, 15, and 40 nm), we examined their subcellular localization in gills and digestive gland. Clams were exposed to AuNPs stabilized with citrate buffer and then diluted in seawater at the concentration of 100 $\mu g L^{-1}$. After 16 days water-borne exposure, using transmission electron microscopy, few particles were observed in gills, distributed as free in the cytoplasm, or associated with vesicles. In the digestive gland, the most striking feature was the presence of individual or small aggregates 40 nm sized within the nuclei colocalized with DNA. Depending on the size, individual or small aggregates (40 nm AuNPs) or more aggregated NPs (5 and 15 nm) were observed, with at least one of the dimensions (40–50 nm) allowing the passage through nuclear pores. Disorganization of chromatin was marked with an increase in filamentous structures. In some parts no chromatin was visible. Moreover, the perinuclear space from nuclei was enlarged in contaminated clams when compared to controls.

Keywords Gold nanoparticles · *Scrobicularia plana* · Transmission electron microscopy · Chromatin

Y. Joubert · J.-F. Pan · P.-E. Buffet (✉) · C. Mouneyrac · C. Amiard-Triquet
Université de Nantes, MMS EA 2160,
LUNAM Université, 9, Rue Bias,
44035 Nantes, France
e-mail: pe.buffet@yahoo.fr

J.-F. Pan
College of Environmental Science and Engineering,
Ocean University of China, Qingdao 266100 China

P.-E. Buffet · C. Mouneyrac
Université Catholique de l'Ouest, MMS EA 2160,
LUNAM Université, 3, Place André Leroy,
49000 Angers, France

P. Pilet
School of dental Surgery, INSERM U791,
1 Place Alexis Ricordeau,
44042 Nantes Cedex 1, France

D. Gilliland
Institute For Health and Consumer Protection European Commission—DG JRC, Via E. Fermi,
19 I-21027 Ispra, VA, Italy

E. Valsami-Jones
School of Geography, Earth and Environmental Sciences,
University of Birmingham, Edgbaston, Birmingham B15 2TT, UK

E. Valsami-Jones
Department of Earth Sciences, Natural History Museum London,
Cromwell Road,
London SW7 5BD, UK

Introduction

Nanotechnology is an emerging field exploiting different materials at the nanometer scale. A wide range of nanomaterials such as iron, silver, carbon, titan, diamond, and gold have been engineered. Among these nanomaterials, nanoparticles (NPs) have been broadly defined as having one size range of 1–100 nm diameter. Due to their size, they have provoked an enormous interest for both industrial and biomedical applications. Gold nanoparticles (AuNPs) show a great potential for cell imaging, targeted drug delivery, cancer diagnostics, and therapeutics. Recently, several groups have demonstrated that AuNPs possess an enormous potential to improve the efficiency of clinical diagnosis [1]

and of cancer treatment [2–5]. As the field continues to develop, the impact of AuNPs on human and environmental health remains unclear. Understanding and controlling the interactions between NPs and living cells will be important for assessing their designated functions since NPs may cause undesirable interactions with biological systems. Moreover, the engineering of large quantities of nanoparticles may lead to unintended contamination of terrestrial and aquatic ecosystems [6]. Thus, they could also represent a potential source of emerging contaminants in the environment. Only a few studies deal with their behavior or impact on the environment [7–12].

At the nanometric scale, NPs acquire novel physicochemical properties that may influence bioavailability. Size, shape, surface chemistry, stability, concentration, and time of exposure are reported to induce different effects (see reviews [13, 14]. Despite showing little or no cytotoxicity via several standard assays, AuNPs may be internalized in the cells and cause cellular damage (see reviews [13, 15, 16]. Most investigators studied specific nanoparticle interactions with single cellular system in which parameters can be controlled, even though this type of model is artificial. Up to date, no consensus exist in regard with the subcellular location of AuNPs (reviewed in Khlebtsov and Dykman [17]): freely dispersed in cytoplasm [18–20] clustered in vesicles [7, 11, 12, 18, 21, 22]. Some studies showed a high fraction of radioactive AuNPs linked to DNA [23], an aggregation of small AuNPs (2 nm) within the nuclei which were damaged [24], a nuclear fragmentation [25, 26].

The main molecular mechanism of nanotoxicity is the induction of oxidative stress by free radical formation [27]. Recent literature contains conflicting data regarding oxidative stress [7, 13, 28] and cytotoxicity of AuNPs [15, 24, 29]. Tissues have potential defense mechanisms, including intracellular antioxidants and antioxidant enzymes [30] such as glutathione S-transferase (GST), superoxide dismutase (SOD), catalase (CAT), and metallothionein proteins (MTs). Our previous investigations [31] showed that activities/concentration of these biomarkers increased following exposure to AuNPs of different sizes on the marine bivalve *Scrobicularia plana* which is an intertidal deposit-feeder organism widely used in ecotoxicological studies [32, 33]. With regard to these results, in the present study we explored the cellular impact of these gold nanoparticles on *S. plana*. Clams were exposed for 16 days to AuNPs of size 5, 15, and 40 nm initially stabilized in citrate buffer (2.5 mM, pH 6.3; 2.5 mM, pH 6.1; and 0.5 mM, pH 6.9 for 5, 15, and 40 nm AuNPs, respectively) as described by Turkevich et al. [34], then diluted in seawater at a concentration of 100 μg AuL^{-1}, concentration used in our previous work [31]. The goal of this study was to determine the subcellular localization of AuNPs in *S. plana* by using transmission electron microscopy (TEM). AuNPs are electronically dense due to their elevated extinction coefficient that allows their detection by TEM. Targeted organs were gills since in bivalves they are the first organs in contact with particles, and digestive gland as a key organ for metal metabolism.

Methods

Animal collection and acclimation

S. plana with shell length of 2.5 cm were collected from the top 20 cm depth intertidal mudflat in March 2010 from the bay of Bourgneuf, located on the French Atlantic coast (1°59′ 04.80″ W, 47°01′50.35″ N). This area is comparatively low in contaminant bioavailabilities according to the results of the French national biomonitoring network RNO [35]. Then clams were transported to the laboratory in cool boxes covered with seaweeds. They were immediately transferred to aerated seawater and allowed to acclimate to the laboratory conditions for 48 h at the same temperature as in the field (10 °C).

Nanoparticle preparation and characterization

More details on the characterization methods are described in Pan et al. [31]. Briefly, AuNPs of three different sizes were prepared at Joint Research Center, Ispra, Italy as a suspension of 98.5 mgL^{-1} in citrate buffer. Gold nanoparticle suspension was characterized [31] by UV–vis spectroscopy and dynamic light scattering. Following addition of the gold to the seawater, the samples were mixed and agitated for a period of 24 h. Electrostatic charge of nanoparticles were defined in citrate buffer and seawater using a ZetaSizer Nano Zs (Malvern Instruments). Samples were transferred to a zeta cell (Malvern Instruments) and measured at 25 °C using an applied voltage of 150 V. Data are expressed as means ± standard error (SE) performed in five replicates.

Particle size and morphology were characterized using a Jeol JEM 1010 (80 kV) equipped with a camera system (Orius 200w Gatan Inc. USA). For sample preparation carbon-coated copper 200 meshes TEM grid (Agar Scientific, UK) were placed onto a drop of 50 μL of citrate-AuNPs for 1 min, and dried at room temperature. Electron micrographs were digitized and analyzed using a Digital Micrograph (Gatan Inc.). For each sample, the size of 200 particles was measured to obtain histograms of particle size distribution.

Elemental analysis was performed on the grids using an X-ray energy dispersive system (ISIS, Oxford Instruments, England) coupled to the TEM.

Nanoparticle exposure

The nanoparticle semi-static exposures were carried out using pre-filtered natural seawater (0.45 μm), with one

control and three AuNP treatments each containing one size of AuNPs (5, 15, and 40 nm, respectively) as described earlier in Pan et al. [31]. For each of the three sizes, the exposure concentration was 100 $\mu g\,Au\,L^{-1}$. For each condition, clams (n=36) were distributed into three polypropylene tanks, each containing 2.0 L exposure medium (12 individuals per tank). Exposure tests were carried out for 16 days at 10 °C in a dark conditioned cabin to avoid light disturbance of endobenthic bivalves. The experimental media (water and NPs) were renewed every other day to ensure oxygen saturation and readjust NP concentration in the water column. Bivalves remained unfed during the whole experiment (16 days) to eliminate the potential food interference and working with lower toxicant conditions than if conducting a shorter test.

Sample preparation for TEM

Following exposure, for each condition (control and NPs of each different size), three clams were collected from three replicated experimental tanks. The isolated tissues (gills and digestive gland) were cut into small parts to obtain fine pieces. They were rinsed in cold phosphate buffer and placed in a fixing solution of glutaraldehyde (2.5 %) and cacodylate buffer (0.1 M) for 2 h at 4 °C and post-fixed in 1 % osmium tetroxide and cacodylate buffer for 1 h at 4 °C. After fixation, samples were rinsed with cacodylate buffer and dried with increasing concentrations of ethanol and propylene oxide. Samples were embedded in EMBed-812 resin (Agar Scientific, UK) and polymerized. Ultrathin sections were performed with an ultramicrotome (Ultracut E, Leica Microsystems, Germany) for TEM were prepared with a diamond knife (Diatome, Switzerland), collected on copper grids and contrasted with uranyl acetate and lead citrate. Samples were observed using a transmission electron microscope (Jeol JEM 1010, Japan).

Results

Elemental analysis

As shown by Zeta potential analysis, AuNPs were negatively charged when suspended in citrate buffer (mean value for 5, 15, and 40 nm, −70±2 mV) and in seawater −18±5 mV).

The nanosize determined by TEM is reported in Fig. 1a–c. Particle sizes are almost homogeneous with respect to size as indicated by the scale bar of 50 nm. Size distribution reported as histograms were respectively 5.3±1.3, 14.1±1.4, and 31±8 nm. The observations of thin sections in biological tissues described below (Figs. 2, 3, 4, 5, 6, and 7) reveal the presence of NPs showing the same sizes and shape than those described in suspensions (Fig. 1) used for experimental contaminations of bivalves.

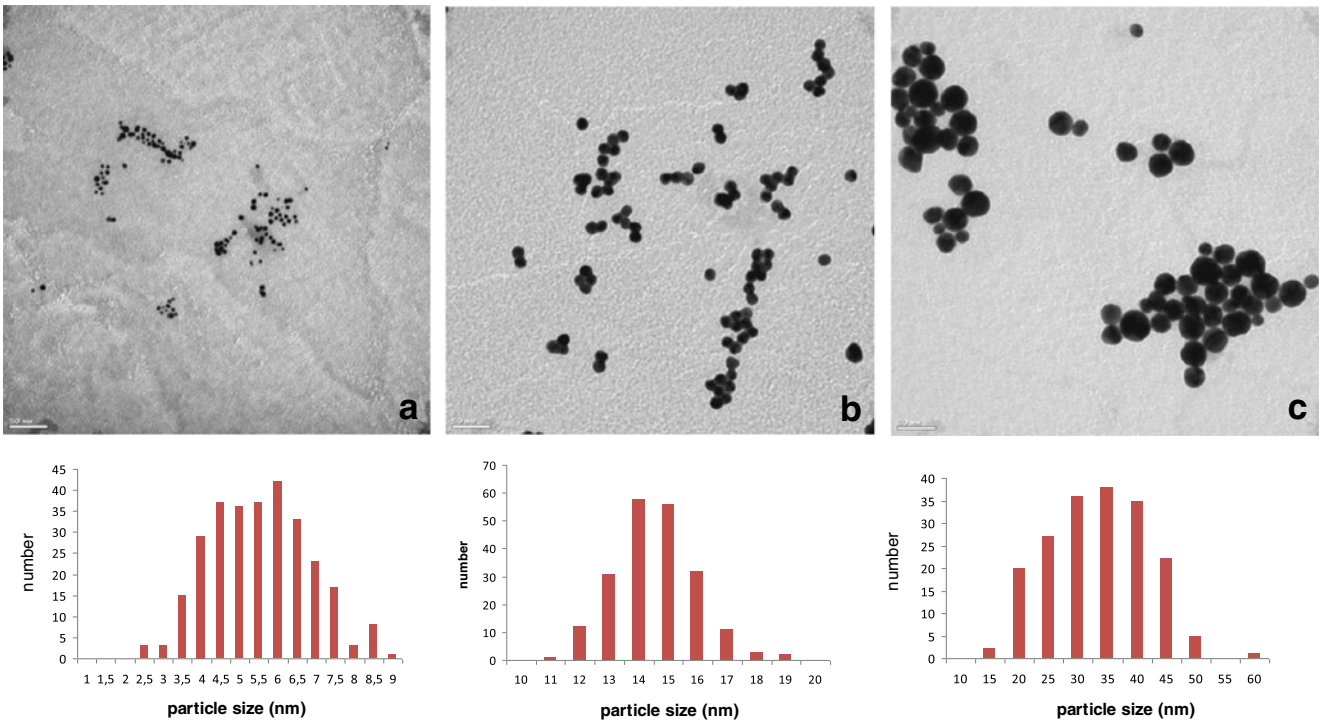

Fig. 1 TEM images of 5 nm (**a**), 15 nm (**b**), and 40 nm (**c**) AuNPs on carbon-coated grids. In each panel, *scale bars* denoting 50 nm and histogram of AuNP diameters determined by analysis of approximately 200 AuNPs located at different regions of the grid

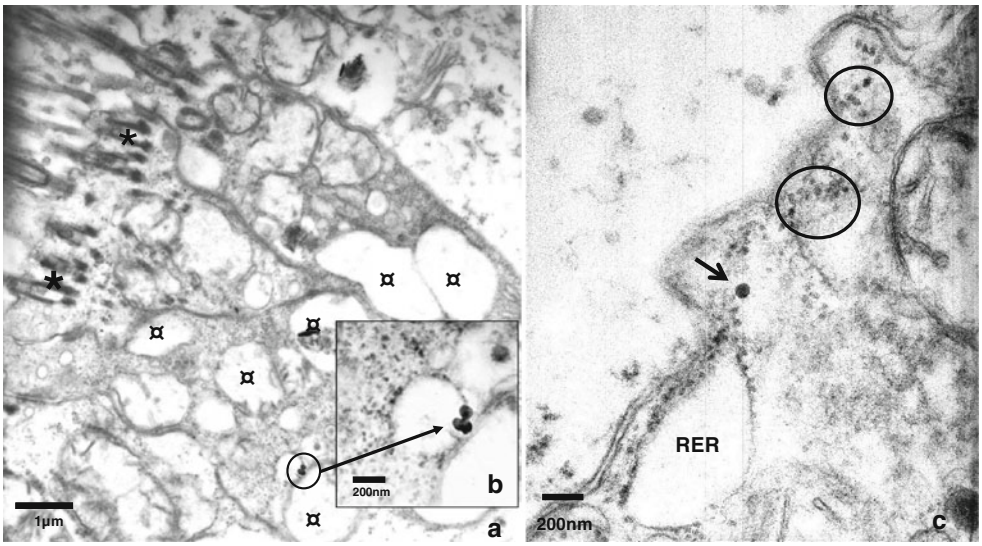

Fig. 2 Electron micrograph of a transverse section through the surface of the border wall of gill in *S. plana*. The presence of cilia (*asterisks*) which penetrate the cytoplasm indicates the apical side of the tissue. **a** localization of 40 nm AuNPs, **b** higher magnification in which three AuNPs are visible. Note the presence of numerous vesicles of different sizes (*currency signs*), **c** localization of a 40 nm AuNP free in the cytoplasm (*arrow*) just near the cell membrane; visualization of rough reticulum endoplasmic (*RER*) and of free ribosomes surrounded by circles in the cytoplasm (*circles*)

Gills

AuNPs were detected close to the basal side of microvilli, therefore demonstrating the ability of AuNPs to penetrate this epithelium (Fig. 2a). Inside the tissue, few particles were found free in the cytoplasm (Fig. 2a, b). Vesicles were more numerous in exposed specimens than observed in controls and their size was highly variable (Fig. 2a). The border wall of microvilli showed no AuNPs retained outside the cell membrane (Fig. 2c). A 40 nm AuNP was visible just near the cell membrane (Fig. 2c). TEM examinations did not reveal any structural disturbance of the plasma membrane. We can observe the rough endoplasmic reticulum (RER) and free ribosomes in the cytoplasm. Since no endocytosis was observed in contaminated gills, TEM examinations cannot give any information about the nature of these vesicles. Although many ultrathin sections from several experimental samples were analyzed, the contamination and the subsequent bioaccumulation of AuNPs in the gills remained still very weak.

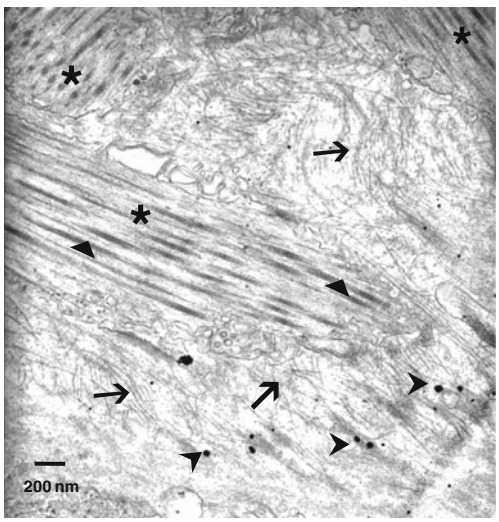

Fig. 3 Electron micrograph through the microvillus border of the digestive gland. Straight microvilli (*asterisks*) are longitudinally oriented and anchored in the apical cytoplasm. The central microvillus core composed of a dense fibrillar meshwork (*triangles*) is surrounded by a microtubule zone (*arrows*) near the apical web. AuNPs (15 nm) are associated with these microtubules (*arrowheads*)

Digestive gland

Electron micrograph of a section through the microvillous border and the apical cytoplasm of the absorptive tissue showed the footlet of a microvillus surrounded by a dense fibrillar meshwork (Fig. 3). These cytoplasmic microtubules shaped a filamentous area out of several microtubules orientated as longitudinal sections. Not a single AuNPs could be observed in contact with the microvilli border outside the plasma membrane. No endocytosis figures (i.e., vesicles formed by invagination of the plasma membrane) were found in the apical plasma membrane. AuNPs were detected close to the basal side near microvilli inside epithelial digestive gland. Unlike AuNPs found in gills, those found in digestive gland were never located inside vesicles.

Exposure to 40 nm AuNPs

When comparing the morphological features between controls and contaminated samples, nuclei contrasted markedly. In controls, chromatin condensed as heterochromatin was distributed all over the nucleus (Fig. 4a). In experimental *S. plana*, TEM examination revealed the localization of 40 nm AuNPs within the nuclei in the digestive gland tissue. Single particles or small clusters of three to five AuNPs were distributed all around the nucleus (Fig. 4b). In clams exposed to AuNPs, visually the amount of heterochromatin was generally less abundant and few amount of chromatin was visible in the central part of the nucleus 1 (Fig. 4b).

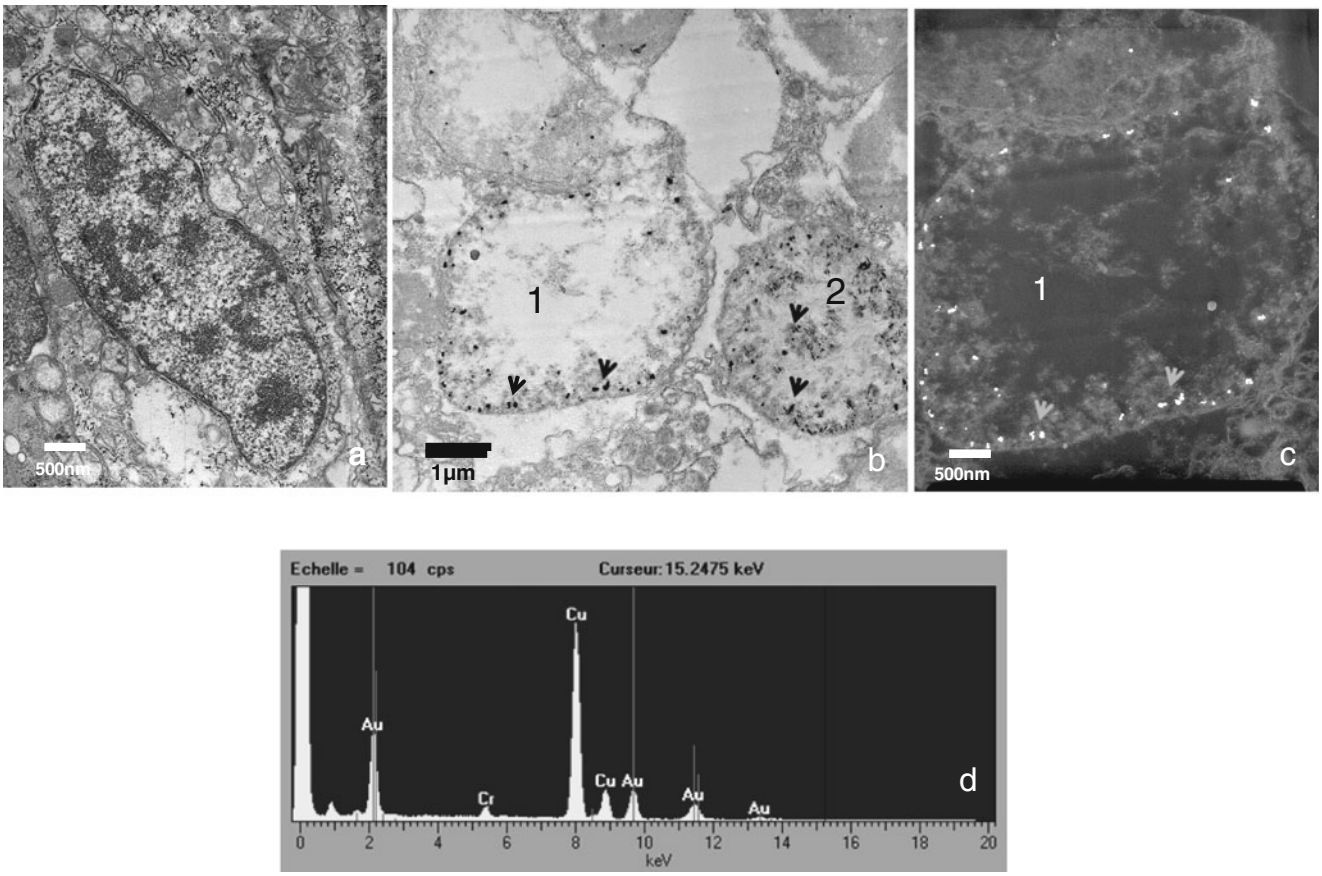

Fig. 4 **a** In controls, chromatin appears as heterochromatin distributed all over the nucleus, **b** in contaminated *S. plana* 40 nm AuNPs are visualized within two nuclei (*1*, *2*), AuNPs are always associated with chromatin (*arrowheads*), the degradation of which seems to be higher in nucleus 1 than in nucleus 2, **c** negative film of the nucleus 1, AuNPs associated with chromatin are more visible and appear as *white dots* (*arrowheads*). **d** Elemental composition of NPs collected through an analysis X by EDS that shows the presence of Au as indicated by the three peaks corresponding to the gold M shell (2.2 keV) and L shells (9.7 and 11.5 keV)

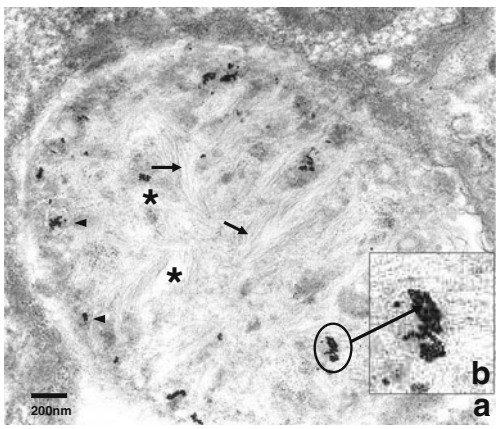

Fig. 5 **a** In contaminated *S. plana*, AuNPs (15 nm) are aggregated to each other. The number of NPs inside these formations seems to be variable (*arrowheads*). They are localized within the chromatin which appears strongly altered. At some places, no more chromatin can be seen (*asterisks*) and fibrillar material was observed instead of condensed chromatin (*arrows*). Nucleus volume is swollen, **b** higher magnification of an AuNP aggregate with an approximate width of 40–50 nm

Everytime, AuNPs were localized in the vicinity of chromatin. However, AuNP uptake within cell nuclei was not homogeneous in the whole tissue. TEM digestive gland cells examination revealed two nuclei invaded by AuNPs (Fig. 4b). Figure c is the negative film from the figure b, in which AuNPs appear as white dots. These nuclei were always visualized within the apical cytoplasm adjacent to the plasma membrane. No endocytosis process was visible at the apical surface. Cytoplasmic membrane, mitochondria, and cytoplasmic reticulum seemed morphologically intact (not shown).

Elemental analysis using an X-ray energy dispersive system on the ultrathin sections (Fig. 4d) proved the presence of Au as indicated by the three peaks corresponding to the gold M shell (2.2 keV) and L shells (9.7 and 11.5 keV).

Exposure to 15 nm AuNPs

As for 40 nm AuNPs, 15 nm AuNPs were mainly located within digestive gland cell nuclei (Fig. 5a) but particles often aggregated up to a number of about 15–20 (Fig. 5b).

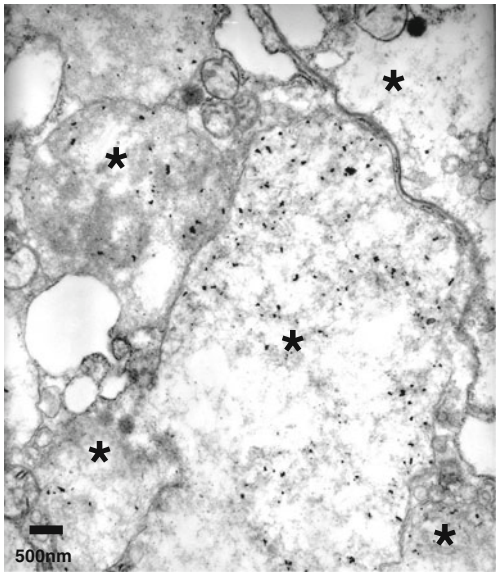

Fig. 6 In contaminated *S. plana*, 15 nm AuNPs are localized within chromatin of several nuclei (*asterisks*) belonging to different cells. The number of contaminated nuclei is higher than that observed with 40 nm AuNPs

At a high magnification, width of aggregates was measured (Fig. 5b). When referred to the scale bar, the width was about 40–50 nm. AuNPs accumulated only in the vicinity of chromatin, the ultrastructure of which was strongly altered compared to controls and 40 nm AuNP exposed tissues. There was less condensed chromatin which seemed to be more dispersed. At some places, fibrillar material was observed instead of condensed chromatin. Moreover, a number of nuclei seemed to be swollen. As in 40 nm AuNPs exposed tissues, nuclei were visualized within the apical cytoplasm (Fig. 6). In the case of 15 nm AuNP exposed tissues, the number of nuclei in which AuNPs were visible, was higher than observed with 40 nm AuNPs (Fig. 6). Aggregated nanoparticles were attached to the microtubules described above (Fig. 3). No endocytosis vacuoles were seen near this terminal web. Although we noticed an increase in intracellular vesicles, there was not AuNPs invasion within these organelles.

Exposure to 5 nm AuNPs

TEM examinations of ultra-thin sections of 5 nm AuNPs exposed epithelial cells of the digestive gland did not reveal any structural disturbance of the plasma membrane, mitochondria, and endoplasmic reticulum (not shown). However, as mentioned previously for 15- and 40-nm AuNP experiments, our results showed the ability of AuNPs to penetrate digestive gland epithelium. Aggregates of AuNPs detected in this tissue remained localized in nuclei (Fig. 7a). Chromatin appeared to be more disorganized than in digestive glands exposed to 15 and 40 nm AuNPs. Chromatin amount was strongly decreased and DNA disorganization extended to the peripheral area (Fig. 7a). We noticed an increase in filamentous structure formation. Therefore, some parts seemed to be devoid of chromatin. AuNPs were condensed into large aggregates which decorated the chromatin. The width of these aggregates was about 40–50 nm (Fig. 7b). The nuclear membrane appeared ruffling (Fig. 7a) and the perinuclear space seemed to be enlarged (Fig. 7a) compared to control (Fig. 7c).

Discussion

As a whole organism is much more complex than a single cell, in vivo toxicological studies are required to assess the safety of nanoparticles. Uptake of AuNPs was shown in the

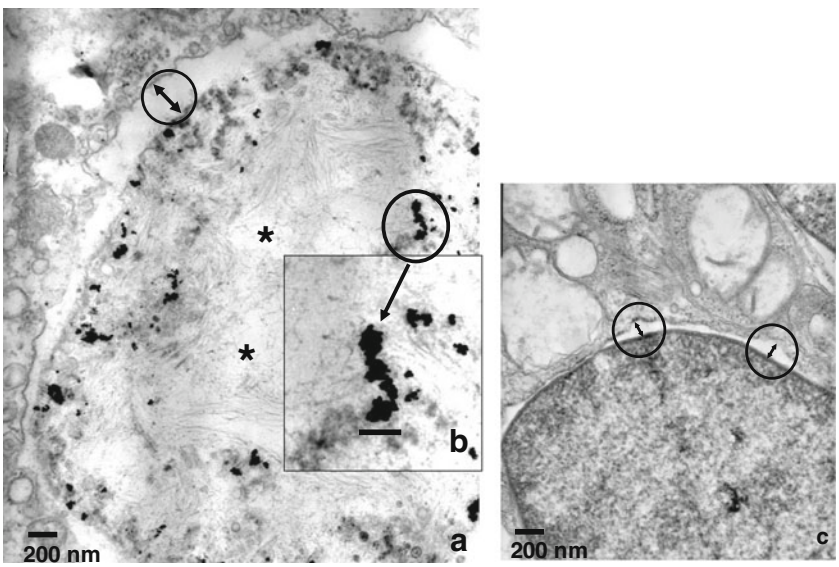

Fig. 7 **a** In contaminated *S. plana*, 5 nm AuNP aggregates with an approximate width of 40–50 nm are localized within chromatin which appears strongly disorganized. That is attested by an increase in filamentous structure. Some parts of the nucleus seem to be devoid of chromatin (*asterisks*), **b** higher magnification of an aggregate. The perinuclear space is enlarged (*up down arrows*) in contaminated *S. plana* (**a**) when compared to the control (**c**). Note the morphological change in chromatin between control (**a**) and contaminated *S. plana* (**b**)

whole soft tissues of the bivalve *S. plana* exposed in vivo to AuNPs of different sizes [31].

The AuNPs examined in the present study have been characterized by Pan et al. [31]. It has been shown that aggregation occurred in seawater for all the three different sizes of AuNPs, increasing from nanosize 5–40 nm to size >700 nm. These findings are in agreement with the loss of charge measured with ZetaSizer for AuNPs (5, 15, and 40 nm) suspended in seawater in the present work, contributing to the aggregation.

The present study reveals that all of these bioaccumulated AuNPs were localized almost exclusively in the digestive gland confirming the results obtained in two other bivalves, namely *Mytilus edulis* [11] and *Corbicula fluminea* [7, 36]. Particulate matter and AuNP aggregates deposited on the bottom of the experimental tank are ingested through the inhalant siphon of the clams, subsequently transported to the mouth, then to the digestive tract and the digestive gland for intracellular digestion [37]. Such a location of AuNPs in digestive gland is not surprising as this organ is known to be a key site of metal detoxification [38].

AuNPs were detected inside digestive epithelium but also inside gill epithelium, demonstrating their ability to cross these barriers. AuNPs had different cellular localization when comparing gills and digestive gland. AuNPs which had penetrated gill cells seemed to be free in the cytoplasm. AuNPs were never observed outside this border and no damage or invagination of the plasma membrane suggesting endocytosis were visible. So, the mechanism allowing AuNPs to enter the cells could not be established from by our observations. However, from several in vitro [16, 19, 39] and in vivo studies [7, 11], it was reported that particles entering cells were trapped in vesicles.

In the digestive gland, once particles have crossed the microvillous border, our TEM observations indicated the presence of AuNPs associated with filaments supporting the apical web near the outer surface, suggesting that AuNPs could be passively transported all along these contractile structures toward the nuclear membrane.

The 40 nm AuNPs entered the digestive gland cells and were exclusively localized within cell nuclei (Fig. 4b and c). In these nuclei, single or two to three aggregates were distributed along the chromatin and seemed to be specially linked to the chromatin. The loss of condensed chromatin is evident, indicating that the condensed DNA of the nucleus had been damaged. No more dense chromatin was observed in some part of the nucleus. Despite this ultrastructural abnormality, mitochondria or plasmic membranes seemed to be still intact. The 15 and 5 nm AuNPs were also localized within the nuclei. However, for these sizes of AuNPs, some striking differences have been noticed. There are only a few single particles linked to chromatin, most of them were aggregated into patches of different sizes. The morphological modifications of chromatin previously mentioned were more pronounced and DNA appeared as fibrillar. AuNPs could be counted and sized within these aggregates. Whatever number of AuNPs in aggregates the shape of them seemed to be defined. When measuring the size of these aggregates, we noticed that the width was always between 40 and 50 nm. As the AuNPs of the three sizes (5, 15, and 40 nm) are able to cross the nuclear membrane, it appears that AuNPs may have pass through the nuclear pores which have a central channel of a patent diameter of 40 nm [40]. Based on this assumption, single 40 nm and aggregates of 5 and 15 nm AuNPs have to be flexible for crossing the nuclear pores. Chitrani et al. [21] showed that the maximum cellular uptake occurred at a nanoparticle size of 50 nm. However, these authors claimed that particles were trapped in vesicles and did not enter the nucleus.

Our previous data [31] showed that in seawater an aggregation occurred for AuNPs of the three sizes. The diameter size of these aggregates was identical and peaked at 600 nm for the three types of NPs. That implies that following uptake, aggregates will be likely broken down by the action of the cilia present all along the gills and on the microvillous border of the digestive gland. Moreover, aggregates could be dissociated chemically in the digestive tract under acid pH 4.5 [41].

In bivalves, bioaccumulation and cytotoxicity of AuNPs was reported by Renault et al. [7] and Tedesco et al. [11, 12] without any clear demonstration of nuclear localization. AuNPs have been found inhibiting cell proliferation by down-regulating cell cycle genes [19]. Panessa-Warren et al. [24] claimed that only small clusters of 2 nm NPs were seen at the nuclear membrane and within the nucleus of lung epithelial cells, whereas, the 10 nm AuNPs were not seen within nuclei. They suggested that the larger core size may not allow their crossing through the nuclear channel measuring 9 nm. But it seems to result from a misinterpretation of the report by Franke et al. [42] indicating a size exclusion limit of approximately 18 nm, whereas a more recent paper [40] indicates a nuclear pore size of 40 nm.

Although NP-induced cytotoxicity has been reported by several groups, many biomedical applications have been reported. Gold NPs conjugated to antibodies can be selectively targeted to cancer cells without significant binding to healthy cells [2, 43]. Gold nanospheres anticancer therapy by using their two-photon absorption of 800 nm laser light was reported by the same group [44]. Recently, Patra et al. [5] have developed a NP-based targeted drug delivery system (DDS) using an anti-epidermal growth factor receptor as a targeting agent, gemcitabine as the anti-cancer drug, and gold as the delivery vehicle in pancreatic cancer. They demonstrated that targeted DDS was much more effective to inhibit the proliferation of pancreatic cancer cells than its

non-targeted counterpart. Kang et al. [4] proposed that AuNPs can be used alone as an anticancer therapeutic material if conjugated to the proper nuclear-targeting ligand such as the nuclear localization signal peptide sequence (NLS). NLS is known to associate with importin-protein in the cytoplasm after which translocation to the nucleus occurs. In this case, AuNPs induces DNA damage, causing cytokenesis arrest and apoptosis [4]. Our results strongly demonstrate that AuNP localization was observed in cell nuclei without any nanogold targeting signal.

Taken together, our results suggested that the three sizes of AuNPs have a capability of inducing DNA damage and subsequent events which can specially affect cellular functions leading to cell death. What kind of cell death AuNPs could induce: necrosis or apoptosis? No fragmentation of nuclei and/or cytoplasmic organelles indicating apoptosis process was visible. Results of Pan et al. [25] concluded to a size-dependent cytotoxicity, in that 1.4 nm particles trigger necrosis by oxidative stress and mitochondrial damage. Our TEM examinations demonstrated a swollen shape of nuclei which could lead to necrosis. That point requires attention because following necrosis, AuNPs could be externalized in the whole tissue and targeted toward other nuclei. In this way, necrosis could spread everywhere. The products released by necrosis process are highly inflammatory and could cause inflammation in the whole animal. AuNPs could be redistributed via the hemolymph as demonstrated by intravenous administration of AuNPs in mice [45, 46]. Nanoparticle exposure induces responses of biomarkers of defense such as MTs, involved in metal detoxification, GST produced in presence of xenobiotics, and SOD and CAT enzymes expressed in oxidative stress [47, 48]. Our parallel study [31] demonstrated that following exposure of *S. plana* to 5, 15, and 40 nm AuNPs, these biomarkers were responsive. As AuNPs are xenobiotics, GST activities highly increased. MT levels were higher in exposed than in control animals. It has been shown that MTs play an important role in metal detoxification in bivalves since they are responsible for the sequestration of metal ions [49]. MTs are also involved in the defense against oxidative stress [38]. The activities of CAT and SOD involved in the primary defenses were increased demonstrating the induction of an oxidative stress by AuNPs. It has been demonstrated that amine-coated AuNPs trigger MT overproduction and an oxidative stress in gills and visceral mass of the bivalve *C. fluminea* during a trophic contamination experiment [7].

The present study suggests morphological alterations of the nuclear membrane in experimental groups compared to controls. TEM observations in controls revealed a thin perinuclear space whereas in contaminated clams this space seemed to be enlarged. In the same way, nuclei shape appeared swollen and amount of condensed chromatin was highly decreased. In addition, a more pronounced alteration was observed following 15 and 5 nm AuNP exposures. Such morphological features could indicate a disturbance of the nuclear membrane due to the induction of oxidative stress by reactive oxygen species which in excess cause protein, DNA, and membrane injury [50, 51]. However, in the absence of any significant increase of thiobarbituric acid-reactive substances, no lipid peroxidation was revealed in *S. plana* [31]. On the other hand, lipid peroxidation products were detected in digestive glands of *M. edulis* exposed to 5 nm AuNPs [11] whereas their previous investigation found no significant increase in tissues of mussels exposed to AuNPs at 13 nm [12].

Taken together, our results demonstrate that the presence of AuNPs is clearly corroborated to a morphological change in chromatin. To our knowledge, only few papers reported a nuclear localization following AuNPs exposure [24].

Conclusions

We have shown that AuNPs at 5, 15, and 40 nm are able to penetrate within branchial and digestive epithelia of a benthic bivalve *S. plana* during a water-borne contamination experiment. Differences between the selective tissue bioaccumulation were observed. In gills, only few AuNPs were observed whereas in digestive glands they were numerous and located within the nuclei whatever the size (5, 15, and 40 nm). According to our previous study [31] demonstrating an increase in biomarker responses linked to oxidative stress, the present study suggests a potential cytotoxicity. Till now, most of the studies suggesting toxicity of AuNPs were based on in vitro experimentation. Our evaluation of toxicity in vivo suggest morphological disturbance of nuclear membrane and chromatin which could lead to a necrosis process. That points out the necessity to investigate the feasibility of minimizing the cytotoxicity of AuNPs before their use in various medical applications without any hazardous effects on human health. Moreover, our results demonstrate uptake and bioaccumulation of AuNPs from an aquatic ecosystem to a marine bivalve. These findings are of interest in a species which plays a major role in the coastal and estuarine food chain since recent reports have brought evidence for transfer of gold particles within a terrestrial food chain [52] and within an estuarine food chain [9]. Despite the doses tested in the present study are too high to be encountered in the environment, the fact that AuNPs may be accumulated within living organisms and the food chain, with potential toxicity at the level of cellular nuclei and chromatin indicates that the use of AuNPs must be developed in a precautionary manner to avoid environmental impacts. Till now, AuNPs were generally considered nontoxic like bulk gold, which is inert and biocompatible.

However, recent findings (this study and literature quoted therein) highlight that there is an urgent need to better understand their nanotoxicity.

Acknowledgments This work was supported by a post-doctoral scholarship from the Fondation Franco-Chinoise pour la Science des Applications (FFCSA), China Scholarship Council (CSC), and the Région Pays de la Loire. We kindly thank Prof. Jacques Taxi (UM 74, Université Pierre et Marie Curie, Paris) for helpful discussions and Hélène Terisse (Institut des Matériaux, Nantes) for Zetapotential analyzer. We also acknowledge INSERM U791 for facilities to TEM access. The authors thank the NanoReTox program (part of the EC FP7/2007-2013) for providing contaminated bivalves.

References

1. Baptista P, Pereira E, Eaton P, Doria G, Miranda A, Gomes I, Quaresma P, Franco R (2008) Gold nanoparticles for the development of clinical diagnosis methods. Anal Bioanal Chem 391:943–950
2. El-Sayed IH, Huang X, El-Sayed MA (2006) Selective laser photothermal therapy of epithelial carcinoma using anti-EGFR antibody conjugated gold nanoparticles. Cancer Lett 239:129–135
3. Panyala NR, Pena-Méndez EM, Havel J (2009) Gold and nano-gold in medicine: overview, toxicology and perspectives. J Appl Biomed 7:75–91
4. Kang B, Mackey MA, EL-Sayed MA (2010) Nuclear targeting of gold nanoparticles in cancer cells induces DNA damage, causing cytokinesis arrest and apoptosis. J Am Soc 132:1517–1519
5. Patra CR, Bhattacharya R, Mukhopadhyay D (2010) Fabrication of gold nanoparticles for targeted therapy in pancreatic cancer. Adv Drug Deliv Rev 62:346–361
6. Klaine SJ, Alvarez PJJ, Batley GE, Fernandez TF, Handy RD, Lyon DY, Mahendra S, McLaughlin MJ, Lead JR (2008) Nanomaterials in the environment: behavior, fate, bioavailability, and effects. Environ Toxicol Chem 27:1825–1851
7. Renault S, Baudrimont M, Mesmer-Dudon N, Gonzales P, Mornet S, Brisson A (2008) Impact of gold nanoparticle exposure on two freshwater species a phytoplanctonic alga (*Scenedesmus subspicatus*) and benthic bivalve (*Corbicula fluminea*). Gold Bulletin 41(2):116–126
8. Farkas J, Christian P, Urrea JAG, Roos N, Hassellôv M, Tollefsen KE, Thomas KV (2009) Effects of silver and gold particles on rainbow trout (*Oncorhynchus mykiss*) hepatocytes. Aquat Toxicol 96:44–52
9. Ferry JL, Craig P, Hexel C, Sisco P, Frey R, Pennington PL, Fulton MH, Scott IG, Decho AW, Kashiwada S, Murphy CJ, Shaw TJ (2009) Transfer of gold nanoparticles from the water column to the estuarine food web. Nature Nanotech 4:441–444
10. Ward JE, Kach DJ (2009) Marine aggregates facilitate ingestion of nanoparticles by suspension-feeding bivalves. Mar Environ Res 68:137–142
11. Tedesco S, Doyle H, Blasco J, Redmond G (2010) Oxidative stress and toxicity of gold nanoparticles in *Mytilus edulis*. Aquat Toxicol 100:178–186
12. Tedesco S, Doyle H, Blasco J, Redmond G, Sheehan D (2010) Exposure of the blue mussel, *Mytilus edulis*, to gold nanoparticles and the pro-oxidant menadione. Comp Biochem Physiol C: Pharmacol Toxicol 151:167–174
13. Lewinsky N, Colvin V, Drezek R (2008) Cytotoxicity of nanoparticles. Small 4:26–49
14. Levy R, Shaheen U, Cesbron Y, Sée V (2010) Gold nanoparticles delivery in mammalian live cells: critical review. Nano Reviews 1:4889
15. Murphy CJ, Gole AM, Stone JW, Sisco PN, Alkilany AM, Goldsmith EC, Baxter SC (2008) Gold nanoparticles in biology: beyond toxicity to cellular imaging. Accounts Chem Res 41:1721–1730
16. Alkilany AM, Murphy CJ (2010) Toxicity and cellular uptake of gold nanoparticles: what we have learned so far? J Nanopart Res 12:2313–2333
17. Khlebtsov N, Dykman L (2010) Biodistribution and toxicity of engineered gold nanoparticles: a review of in vitro and in vivo studies. Chem Soc Rev 40:1647–1671
18. Nativo P, Prior IA, Brust M (2008) Uptake and intracellular fate of surface-modified gold nanoparticles. Acs Nano 8:1639–1644
19. Li JJ, Zou L, Hartono D, Ong CN, Bay BH, Lanry Yung LY (2008) Gold nanoparticles induce oxidative damage in lung fibroblasts in vitro. Adv Mater 20:138–142
20. Stelzer R, Hutz RJ (2009) Gold nanoparticles enter rat ovarian granulosa cells and subcellular organelles, and alter in-vitro estrogen accumulation. J Reprod Dev 55:685–690
21. Chitrani BD, Ghazani AA, Chan WCW (2006) Determining the size and shape dependence of gold nanoparticle uptake into mammalian cells. Nano Lett 6:662–668
22. Pernodet N, Fang X, Sun Y, Bakhtina A, Ramakrishnan A, Sokolov J, Ulman A, Rafailovich M (2006) Adverse effects of citrate/gold nanoparticles on human dermal fibroblasts. Small 6:766–773
23. Tsoli M, Kuhn H, Brandau W, Esche H, Schmid G (2005) Cellular uptake and toxicity of Au55 clusters. Small 1:841–844
24. Panessa-Warren BJ, Warren JB, Maye MM, Van der Lelie D, Gang O, Wong S, Ghebrehiwet B, Tortora GT, Misewich JA (2008) Human epithelial cell processing of carbon and gold nanoparticles. Int J Nanotechnol 5:55–91
25. Pan YS, Neuss LA, Fischler M, Wen F, Simon U, Schmid G, Brandau W, Jahen-Dechent W (2007) Size-dependent cytotoxicity of gold nanoparticles. Small 11:1941–1949
26. Patra HK, Banerjee S, Chaudhuri U, Lahiri P, Dasgupta AK (2007) Cell selective response to gold nanoparticles. Nanomedicine 3:111–119
27. Lanone S, Boczkowski J (2006) Biomedical applications and potential health risks of nanomaterials: molecular mechanisms. Curr Mol Med 6:651–663
28. Tedesco S, Doyle H, Redmond G, Sheehan D (2008) Gold nanoparticles and oxidative stress in *Mytilus edulis*. Mar Environ Res 66:131–133
29. Cho WS, Cho MJ, Jeong J, Choi M, Cho HY, Han BS, Kim SH, Kim HO, Lim YT, Chung BH, Jeong J (2009) Acute toxicity and pharmacokinetics of 13 nm-sized PEG-coated gold nanoparticlesToxicol. Appl Pharmacol 236:16–24
30. Young IS, Woodside JV (2001) Antioxidants in health and disease J Clin Pathol 54:176–186
31. Pan JF, Buffet PE, Poirier L, Amiard-Triquet C, Gilliland D, Guibbolini M, Christine C, Roméo M, Mouneyrac C (2012) Size dependent bioaccumulation and ecotoxicity of gold nanoparticles in an endobenthic invertebrate: the tellinid clam *Scrobicularia plana*. Environ Poll 168:37–43
32. Bonnard M, Roméo M, Amiard-Triquet C (2009) Effects of copper on the burrowing behavior of estuarine ans costal invertebrates, the polychaete *Nereis diversicolor* and the bivalve *Scrobicularia plana*. Hum Ecol Risk Assess 15:11–26
33. Solé M, Kopecka-Pilarczyk J, Blasco J (2009) Pollution biomarkers in two estuarine invertebrates, *Nereis diversicolor* and

Scrobicularia plana, from a Marsh ecosystem in SW Spain. Environ Int 35:523–531
34. Turkevich J, Stevenson PC, Hillier JA (1951) Study of the nucleation and growth processes in the synthesis of colloidal gold. Discuss Faraday Soc 11:55–59
35. RNO (2006) Surveillance de la qualité du milieu marin Ministère de l'environnement et Institut français de recherche pour l'exploitation de la mer (Ifremer), Paris et Nantes
36. Hull MS, Chaurand P, Rose J, Auffan M, Bottero JY, Jones JC, SchultzIR VPJ (2011) Filter-feeding bivalves store and biodeposit colloidally stable gold nanoparticles. Environ Sci Technol 45:6592–6599
37. Hughes RN (1969) A study of feeding in *Scrobicularia plana*. J Mar Biol Assoc UK 49:805–823
38. Viarengo A, Burlando B, Cavaletto M, Marchi B, Ponzano E, Blasco J (1999) Role of metallothionein against oxidative stress in the mussel *Mytilus galloprovincialis*. AMJ Physiol Reg Integr Comp Physiol 277:R1612–1619
39. Peckys DB, de Jonge N (2011) Visualizing gold nanoparticle uptake in live cells with liquid scanning transmission electron miscroscopy. Nano Lett 11:1733–1738
40. Jovanovic-Talisman T, Tetenbaum-Novatt J, McKenney AS, Zilman A, Peter R, Rout MP, Chait BT (2009) Artificial nanopores that mimic the transport selectivity of the nuclear pore complex. Nature 457:1023–1027
41. Payne DW, Thorpe NA (1993) Carbohydrate digestion in the bivalve *Scrobicularia plana* (da costa). Comp Biochem Physiol 104B:499–503
42. Franke WW, Scheer U, Krohne G, Jarasch ED (1981) The nuclear envelope and the architecture of the nuclear periphery. J Cell Biol 1(91):39s–50s
43. Huang X, El-Sayed EH, Quian W, El-Sayed MA (2006) Cancer cell imaging and photothermal therapy in the near-infrared region by using gold nanorods. J Am Chem Soc 128:2115–2120
44. Jain PK, Huang X, El-Sayed HI, El-Sayed MA (2008) Noble metals on the nanoscale: optical and photothermal properties and some applications in imaging, sensing, biology, and medicine. Acc Chem Res 41:1578–1586
45. De Jong WH, Hagens WL, Krysteck P, Burger MC, Sips AJAM, Geertsma RE (2008) Particle size-dependent organ distribution of gold nanoparticles after intravenous administration. Biomaterials 29:1912–1919
46. Sonavane G, Tomoda K, Makino K (2008) Biodistribution of colloidal gold nanoparticles after intravenous administration: effect of particle size. Colloids Surf B: Biointerf 66:274–280
47. Van der Oost R, Porte-Visa C, Van den Brink NW (2005) Ecotoxicological testing of marine and freshwater ecosystems. In: Munawar M (ed) P J Den Besten. Taylor and Francis, Boca Raton, pp 87–152
48. Marquis BJ, Love SA, Braun KL, Haynes CL (2009) Analytical Methods to Assess Nanoparticle Toxicity Analyst 134:425–439
49. Amiard JC, Amiard-Triquet A, Barka S, Pellerin S, Rainbow PS (2006) Metallothioneins in aquatic invertebrates: their role in metal detoxification and their use as biomarkers. Aquat Toxicol 76:160–202
50. Nel A, Xia T, Mädler L, Li N (2006) Toxic potential of materials at the nanolevel. Science 311:622–627
51. Aillon KL, Xie Y, El-Gendy N, Berkland CJ, Forres ML (2009) Effects of nanomaterial physicochemical properties on in vivo toxicity. Adv Drug Deliv Rev 61:457–466
52. Judy JD, Unrine JM, Bertsch PM (2011) Evidence for biomagnification of gold nanoparticles within a terrestrial food chain. Environ Sci Technol 45:776–781